Radiomic measures from chest high-resolution computed tomography associated with lung function in sarcoidosis

Sarah M. Ryan[1], Tasha E. Fingerlin[1,2,3], Margaret Mroz[4], Briana Barkes[4], Nabeel Hamzeh[5], Lisa A. Maier[4,6,7] and Nichole E. Carlson[1]

@ERSpublications
Radiomic measures identify pulmonary parenchymal abnormalities in sarcoidosis and are highly associated with lung function, suggesting that radiomics could enhance visual reads and result in improved patient profiling, disease staging and monitoring. http://bit.ly/2HMLaKm

Cite this article as: Ryan SM, Fingerlin TE, Mroz M, *et al*. Radiomic measures from chest high-resolution computed tomography associated with lung function in sarcoidosis. *Eur Respir J* 2019; 54: 1900371 [https://doi.org/10.1183/13993003.00371-2019].

ABSTRACT

Introduction: Pulmonary sarcoidosis is a rare heterogeneous lung disease of unknown aetiology, with limited treatment options. Phenotyping relies on clinical testing including visual scoring of chest radiographs. Objective radiomic measures from high-resolution computed tomography (HRCT) may provide additional information to assess disease status. As the first radiomics analysis in sarcoidosis, we investigate the potential of radiomic measures as biomarkers for sarcoidosis, by assessing 1) differences in HRCT between sarcoidosis subjects and healthy controls, 2) associations between radiomic measures and spirometry, and 3) trends between Scadding stages.

Methods: Radiomic features were computed on HRCT in three anatomical planes. Linear regression compared global radiomic features between sarcoidosis subjects (n=73) and healthy controls (n=78), and identified associations with spirometry. Spatial differences in associations across the lung were investigated using functional data analysis. A subanalysis compared radiomic features between Scadding stages.

Results: Global radiomic measures differed significantly between sarcoidosis subjects and controls ($p<0.001$ for skewness, kurtosis, fractal dimension and Geary's *C*), with differences in spatial radiomics most apparent in superior and lateral regions. In sarcoidosis subjects, there were significant associations between radiomic measures and spirometry, with a large association found between Geary's *C* and forced vital capacity (FVC) ($p=0.008$). Global radiomic measures differed significantly between Scadding stages ($p<0.032$), albeit nonlinearly, with stage IV having more extreme radiomic values. Radiomics explained 71.1% of the variability in FVC compared with 51.4% by Scadding staging alone.

Conclusions: Radiomic HRCT measures objectively differentiate disease abnormalities, associate with lung function and identify trends in Scadding stage, showing promise as quantitative biomarkers for pulmonary sarcoidosis.

This article has supplementary material available from erj.ersjournals.com

Received: 21 Feb 2019 | Accepted after revision: 24 May 2019

Introduction

Pulmonary sarcoidosis is a rare heterogeneous disease of unknown aetiology characterised by the formation of granulomas in the lungs, as well as other organs. Compromised lung function is common with pulmonary involvement [1], which can limit daily activities, and frequently indicates the need for therapy to reduce or reverse abnormalities. Spontaneous remission has been reported to occur in up to two-thirds of patients in certain populations [2], yet mortality rates due to respiratory failure are rising in the USA [3].

Assessment of chest radiography, in addition to lung function, is used to clinically monitor sarcoidosis, with chest radiographs showing abnormalities in 90% of cases [4]. The Scadding system of staging, based on chest radiographs, is a common visual classification for sarcoidosis, dividing the radiographic manifestations into five stages: stage 0 (no radiograph abnormalities), stage I (bilateral hilar lymphadenopathy (BHL)), stage II (pulmonary infiltration with BHL), stage III (pulmonary infiltration without BHL) and stage IV (pulmonary fibrosis with volume loss). Despite the numerical nomenclature, there is no sequential ordering of Scadding stages and subjects may demonstrate abnormalities in multiple stages at various times. Additional chest radiographic patterns may be observed that are not well characterised by Scadding stage, such as small nodular opacities along the bronchovascular bundle, focal consolidation, consolidation of small nodular opacities (conglomerate masses), ground glass and fibrosis, among others [2].

Recently, high-resolution computed tomography (HRCT) scans have been used to characterise pulmonary sarcoidosis manifestations [5–7]. Despite limited standard visual assessment tools for HRCT sarcoidosis manifestations [8–10], HRCT findings are still characterised visually, which is time consuming, dependent on the expertise of the reader and subject to poor inter-rater reliability [11]. Quantitative assessment of HRCT in sarcoidosis may provide a more rapid, objective and sensitive quantification of the various abnormalities that present in sarcoidosis.

Radiomics, an emerging field in which large numbers of quantitative imaging features are computed from medical images, has proved useful for developing quantitative biomarkers in emphysema [12–15], interstitial lung disease [16–18] and lung cancer [19–23]. To the best of our knowledge, radiomic measures have yet to be explored in sarcoidosis. Given the usefulness of radiomics in other diseases, we hypothesise that radiomic features will also prove useful as potential imaging biomarkers for sarcoidosis.

Here, we perform an early-stage investigation of radiomic measures as potential biomarkers in sarcoidosis, where "early stage" references the biomarker study pipeline suggested by Pepe *et al.* [24]. Our goal is to investigate whether specific radiomic features on lung HRCT differ between sarcoidosis subjects and healthy controls (figure 1 and table 1). In particular, we compute global and spatially varying radiomic features, and assess how these measures differentiate sarcoidosis subjects from healthy controls and between Scadding stages. Lastly, we relate radiomics and lung function to show the potential of radiomic measures as biomarkers for sarcoidosis.

Methods

Study populations and data acquisition

Supplementary section E1 includes a detailed description of the study populations and imaging acquisition. In brief, the sarcoidosis population (n=79) was recruited at National Jewish Health (Denver, CO, USA) as part of the National Heart, Lung, and Blood Institute-funded Genomic Research in Alpha-1 Antitrypsin Deficiency and Sarcoidosis (GRADS) study [25]. A nonsmoking, healthy control population (n=108) was obtained from the COPDGene study [26]. Subjects in GRADS were 18–85 years old with a confirmed diagnosis of sarcoidosis *via* biopsy or manifestations consistent with acute sarcoidosis (Löfgren's syndrome) [25]. Subjects in the COPDGene study were 45–80 years old with no history of lung disease and normal post-bronchodilator (BD) spirometry [27]. In both GRADS and COPDGene, pulmonary function testing was performed (including pre-BD forced expiratory volume in 1 s (FEV_1) and forced vital capacity (FVC)) and a chest HRCT ordered according to the same imaging protocol [26], except for a difference in tube current average (GRADS: 180–330 mA varied by body mass index (BMI); COPDGene: 400 mA). According to Mackin *et al.* [28], we do not believe the difference in tube current will affect our

Affiliations: [1]Dept of Biostatistics and Informatics, Colorado School of Public Health, Aurora, CO, USA. [2]Dept of Epidemiology, Colorado School of Public Health, Aurora, CO, USA. [3]Dept of Biomedical Research, National Jewish Health, Denver, CO, USA. [4]Dept of Medicine, National Jewish Health, Denver, CO, USA. [5]Dept of Internal Medicine, University of Iowa Hospitals and Clinics, Iowa City, IA, USA. [6]Dept of Medicine, University of Colorado, Denver, CO, USA. [7]Dept of Environmental and Occupational Health, Colorado School of Public Health, Aurora, CO, USA.

Correspondence: Sarah M. Ryan, Dept of Biostatistics and Informatics, Colorado School of Public Health, 17001 E. 17th Place, Aurora, CO 80045, USA. E-mail: sarah.m.ryan@cuanschutz.edu

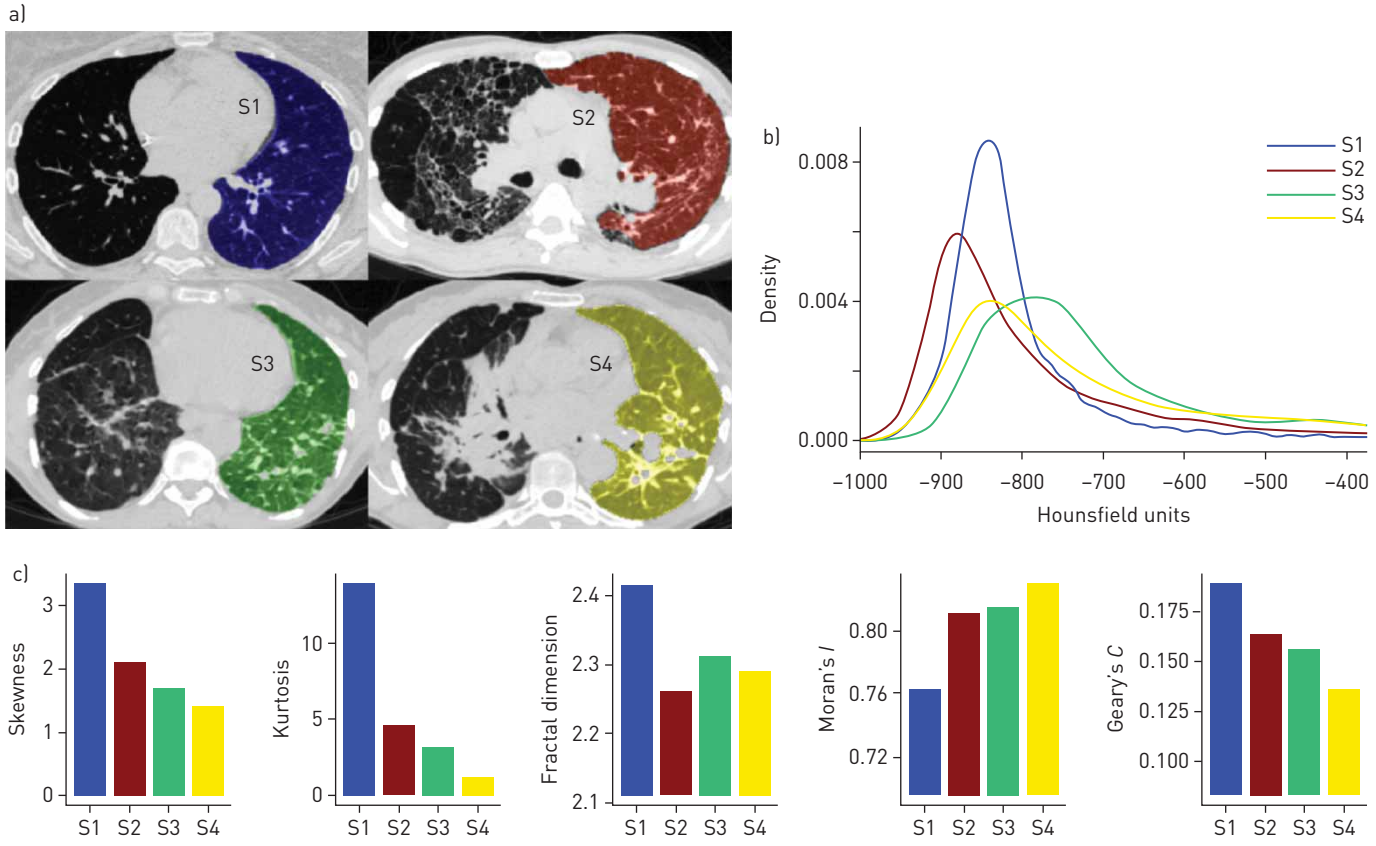

FIGURE 1 a) Representative high-resolution computed tomography (HRCT) scans from subjects S1–S4 representative of HRCT abnormalities, including no abnormalities (S1), mosaic attenuation/honeycombing (S2), nodules (S3) and fibrosis (S4). In general, a two-dimensional HRCT slice from a healthy control subject (S1) appears to have mostly healthy lung tissue, with the occasional blood vessel or airway on the slice. Conversely, the HRCT slices from sarcoidosis subjects (S2–S4) have increased opacification and parenchymal abnormalities apparent, shown by the whiter areas on the HRCT scans. b) These parenchymal abnormalities on the HRCT scans for subjects S2–S4 alter the appearance of the Hounsfield unit histogram, resulting in less skewness and less kurtosis ("peaked") densities compared with the healthy control S1. c) Furthermore, the spatial radiomic measures also differ, with sarcoidosis subjects having smaller fractal dimension and Geary's *C*, and larger Moran's *I*, compared with the healthy control.

results. 73 of the GRADS subjects had HRCT. Only COPDGene subjects scanned on machines from the same manufacturer (Siemens) as the GRADS subjects were analysed in this study (n=78). All subjects provided signed informed consent through either the GRADS or COPDGene studies.

Radiomic measures

Image data pre-processing and radiomics are described in supplementary sections E2 and E3. In brief, lung segmentation and radiomic calculations were performed using the lungct R package (https://github.com/ryansar/lungct). Five radiomic measures (skewness, kurtosis, fractal dimension [29], Moran's *I* [30] and Geary's *C* [31]) were pre-selected for evaluation in our study based on their statistical properties and success in previous studies for idiopathic pulmonary fibrosis and lung nodules [20, 32, 33]. The five radiomic measures were computed on every slice for every subject in each of the two lungs and three anatomical planes. To summarise the distribution of the radiomic features obtained for each subject, lung and plane, the median value was computed. Detailed descriptions of each measure along with directional clinical hypotheses for each measure can be found in figure 1 and table 1.

Statistical analysis

A detailed statistical analysis can be found in supplementary section E4. Descriptive statistics (*e.g.* mean and standard deviation for continuous variables; frequencies for categorical variables) were used to summarise demographic, radiomic and spirometry data (table 2). Linear regression models were used to test for differences in global radiomic measures between sarcoidosis subjects and controls, adjusted for age, sex and BMI (table 3, and supplementary tables E1 and E2). To evaluate whether disease status (*i.e.* sarcoidosis *versus* control) alters associations between lung function and global radiomic measures, linear regressions were fitted with an interaction between disease group and a global radiomic measure (figure 2,

TABLE 1 Description of radiomic features for two-dimensional high-resolution computed tomography (HRCT) slices

Measure and equation[#]	Description	Clinical hypothesis
Skewness $\frac{\frac{1}{n}\sum_{i=1}^{n}(x_i-\bar{x})^3}{\left[\frac{1}{n-1}\sum_{i=1}^{n}(x_i-\bar{x})^2\right]^{\frac{3}{2}}}$	First-order histogram feature that measures the asymmetry of a sample distribution. Positive values indicate right skew, or a long right tail. Values closer to 0 indicate little or no skew.	Sarcoidosis results in increased opacification (*i.e.* whiter regions) on HRCT from parenchymal abnormalities. This will alter the properties of the histogram of Hounsfield units to appear more normally distributed (*i.e.* less skew and less kurtosis). Thus, we hypothesise that sarcoidosis subjects will have less skewness and less kurtosis compared with healthy controls.
Kurtosis $\frac{\frac{1}{n}\sum_{i=1}^{n}(x_i-\bar{x})^4}{\left[\frac{1}{n}\sum_{i=1}^{n}(x_i-\bar{x})^2\right]^2}-3$	First-order histogram feature that measures the tailed-ness of a sample distribution. Positive values indicate infrequent, extreme outliers. Smaller values indicate fewer, less extreme outliers.	
Fractal dimension $1+\text{median}\left[2-\frac{\log V(2)-\log V(1)}{\log 2}\right]$ $V(k)=\frac{\sum_{i=1}^{n}\sum_{j=1}^{n}w_{i,j}(k)\lvert x_i-x_j\rvert}{\sum_{i=1}^{n}\sum_{j=1}^{n}w_{i,j}(k)}$	Second-order texture feature that measures the self-similarity of pixels in space, or the image roughness [29]. On a two-dimensional plane, it ranges from 2 to 3, with lower values indicative of adjacent pixels appearing more similar (*i.e.* more smoothness).	Sarcoidosis involves the formation of micronodules in the lung that may conglomerate as disease worsens, and/or fibrosis may develop. Conglomeration and fibrosis are both represented by adjacent pixels of higher opacification on HRCT (*i.e.* more smoothness). Thus, we hypothesise that sarcoidosis subjects will have lower fractal dimension, higher Moran's *I* and lower Geary's *C* compared with healthy controls.
Moran's I $\frac{n\sum_{i=1}^{n}\sum_{j=1}^{n}w_{i,j}(x_i-\bar{x})(x_j-\bar{x})}{\sum_{i=1}^{n}\sum_{j=1}^{n}w_{i,j}(1)\sum_{i=1}^{n}(x_i-\bar{x})^2}$	Second-order spatial feature that measures global spatial autocorrelation, or similarity of pixels in space [30]. It ranges approximately from −1 to 1, with values around 0 indicative of no spatial autocorrelation and higher values indicative of positive spatial autocorrelation, or adjacent pixels appearing more similar.	
Geary's C $\frac{n\sum_{i=1}^{n}\sum_{j=1}^{n}w_{i,j}(x_i-x_j)^2}{\sum_{i=1}^{n}\sum_{j=1}^{n}w_{i,j}(1)\sum_{i=1}^{n}(x_i-\bar{x})^2}$	Second-order spatial feature that measures local spatial autocorrelation [31]. Geary's *C*, ranging from 0 to 2, is inversely proportional to Moran's *I*, with values close to 0 indicating strong positive spatial autocorrelation, or adjacent pixels appearing more similar.	

[#]: x_i is the Hounsfield unit intensity at a single pixel i; n is the total number of pixels and $\bar{x}$ is the mean Hounsfield units from a lung-masked HRCT slice; $w_{i,j}(k)$ is an indicator function for whether the distance between pixels i and j is k units.

and supplementary tables E3 and E4). In secondary analyses, functional regressions using penalised smoothing splines [34] were fitted to determine whether there was a spatially varying association between subjects with and without sarcoidosis and a radiomic measure, *i.e.* whether certain regions of the lung were more different between sarcoidosis subjects and controls than other regions (figures 3 and 4, and supplementary figures E1 and E2). The analyses were repeated in sarcoidosis subjects to investigate

TABLE 2 Differences in subject characteristics between the control and sarcoidosis populations, and by Scadding stage

	Control	Sarcoidosis	p-value	Stage 0	Stage I	Stage II	Stage III	Stage IV	p-value
Subjects	78	73		9	8	28	11	17	
Male	28 (35.9)	36 (49.3)	0.133	2 (22.2)	3 (37.5)	14 (50.0)	7 (63.6)	10 (58.8)	0.329
White	77 (98.7)	62 (84.9)	0.002	7 (77.8)	8 (100.0)	24 (85.7)	11 (100.0)	12 (70.6)	0.166
Age years	64.51±8.32	54.14±8.64	<0.001	51.44±7.19	52.27±13.79	53.76±9.31	56.93±6.81	55.28±6.24	0.612
BMI kg·m^{-2}	27.97±4.76	30.12±6.95	0.029	36.68±7.20	29.80±5.99	28.55±5.72	30.28±8.74	29.27±6.58	0.040
Pre-BD FEV$_1$ L	2.76±0.71	2.81±0.95	<0.001	2.86±0.85	2.98±1.07	2.85±1.05	3.02±0.80	2.39±0.82	0.055
Pre-BD FVC L	3.61±0.90	3.72±1.20	<0.001	3.45±1.03	3.69±1.31	3.87±1.40	3.92±1.06	3.43±0.95	0.140
FEV$_1$/FVC	0.77±0.05	0.75±0.09	0.465	0.83±0.03	0.81±0.08	0.74±0.08	0.78±0.06	0.68±0.10	<0.001

Data are presented as n, n (%) or mean±SD, unless otherwise stated. BMI: body mass index; BD: bronchodilator; FEV$_1$: forced expiratory volume in 1 s; FVC: forced vital capacity. p-values for lung function measures (pre-BD FEV$_1$, FVC and FEV$_1$/FVC) are adjusted for sex, age, race, ethnicity and height. p<0.05 considered significant.

TABLE 3 Differences in global radiomic features between the control and sarcoidosis populations, and by Scadding stage in the left lung, axial plane

	Control	Sarcoidosis	p-value	Stage 0	Stage I	Stage II	Stage III	Stage IV	p-value
Subjects	78	73		9	8	28	11	17	
Skewness	3.642±0.060	3.166±0.085	<0.001	3.009±0.131	3.491±0.198	3.309±0.150	3.373±0.187	2.727±0.172	0.027
Kurtosis	16.653±0.600	12.732±0.688	<0.001	10.879±1.102	15.052±2.003	14.084±1.259	14.248±1.741	9.413±1.066	0.032
Fractal dimension	2.429±0.003	2.404±0.004	<0.001	2.434±0.011	2.437±0.006	2.397±0.004	2.421±0.005	2.374±0.008	<0.001
Moran's *I*	0.691±0.004	0.702±0.005	0.047	0.667±0.013	0.668±0.013	0.715±0.005	0.680±0.007	0.729±0.008	<0.001
Geary's *C*	0.226±0.002	0.212±0.002	<0.001	0.226±0.006	0.227±0.005	0.208±0.003	0.229±0.005	0.195±0.002	<0.001

Data are presented as n or mean±SE, unless otherwise stated. p-values are adjusted for sex, age and body mass index. p<0.05 considered significant. For right lung and coronal and sagittal results, see supplementary tables E1 and E2.

potential trends in radiomic and lung function measures across Scadding stages. Results were considered significant at p<0.05.

Results

For brevity, the results presented here are for the left lung axial orientation, unless otherwise noted. In general, similar patterns were seen for the right lung, and coronal and sagittal anatomical planes (see supplementary material for more information).

Differences in nonradiomic characteristics between sarcoidosis subjects and controls, and across Scadding stages in sarcoidosis

Table 2 shows the characteristics of the subject population in this study. Compared with controls (n=78), sarcoidosis subjects (n=73) were younger (mean±SD 54.1±8.6 *versus* 64.5±8.3 years; p<0.001), with a higher BMI (mean±SD 30.1±7.0 *versus* 28.0±4.8 $kg \cdot m^{-2}$; p=0.029), larger population of White (84.9% *versus* 94.1%; p=0.002) and a meaningfully, but not significantly, higher percentage of males (49.3% *versus* 35.9%; p=0.133). Adjusted for sex, race, ethnicity, age and height, sarcoidosis subjects had significantly lower pre-BD FEV_1 and FVC (p<0.001 for both) compared with controls, but a similar FEV_1/FVC (p=0.465).

Subject characteristics were similar across the Scadding stages (p>0.05) (table 2), with differences observed in BMI and FEV_1/FVC (p=0.040 and p<0.001, respectively). Stage IV had the lowest FEV_1/FVC, while others had FEV_1/FVC within a normal range.

Differences in global radiomic measures were observed between sarcoidosis subjects and controls

The mean±SE of the global skewness was positive, but lower in sarcoidosis subjects compared with controls (3.17±0.09 *versus* 3.64±0.06; p<0.001), as was the global kurtosis (12.7±0.7 *versus* 16.7±0.6; p<0.001), global fractal dimension (2.404±0.004 *versus* 2.429±0.003; p<0.001) and global Geary's *C* (0.212±0.002 *versus* 0.226±0.002); the global Moran's *I* (mean±SE 0.702±0.005 *versus* 0.691±0.004) was higher in sarcoidosis subjects (p<0.001) (table 3, and supplementary tables E1 and E2).

Associations were apparent between global radiomic measures and lung function, and differed between sarcoidosis subjects and controls

Kurtosis

The relationship between kurtosis and pre-BD FEV_1 (figure 2a) differed between sarcoidosis subjects and controls (p=0.032); in sarcoidosis subjects there was a positive association between kurtosis and FEV_1 (β±SE 0.053±0.012 L; p<0.001); however, in controls there was no significant association between kurtosis and FEV_1 (p=0.189). The relationship between kurtosis and FVC and FEV_1/FVC was positive (figure 2b and c), and did not differ between sarcoidosis subjects and controls (p>0.087).

Geary's C

The association between Geary's *C* and pre-BD FEV_1 (figure 2d), pre-BD FVC (figure 2e) and FEV_1/FVC (figure 2f) differed between sarcoidosis subjects and controls (p<0.001, p=0.002 and p<0.001, respectively); in sarcoidosis subjects there were significant positive associations between Geary's *C* and FEV_1, FVC and FEV_1/FVC (FEV_1: β±SE 15.7±3.6 L; p<0.001; FVC: β±SE 21.4±4.6 L; p=0.008; FEV_1/FVC: β±SE 2.11±0.42; p<0.001); however, in controls there were significant negative associations between Geary's *C* and FEV_1 and FEV_1/FVC (FEV_1: β±SE −10.9±4.5 L; p=0.016; FEV_1/FVC: β±SE −1.06±0.51; p=0.040).

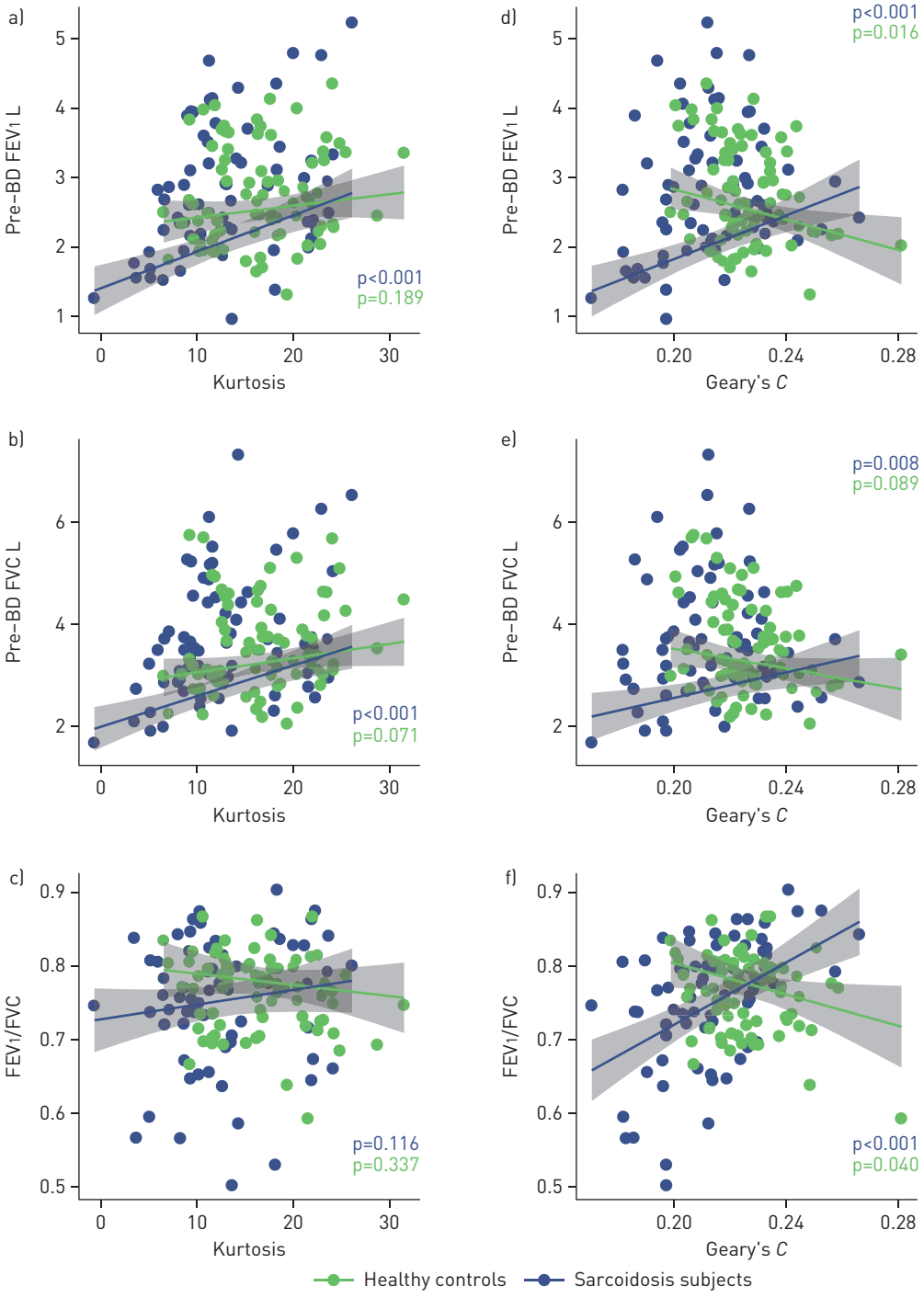

FIGURE 2 Association between lung function and global radiomic features by disease status, adjusted for sex, age and body mass index (BMI). BD: bronchodilator; FEV_1: forced expiratory volume in 1 s; FVC: forced vital capacity. a–c) Kurtosis and d–f) Geary's *C*. a, d) Pre-BD FEV_1, b, e) pre-BD FVC and c, f) FEV_1/FVC. p-values test for significant associations between lung function and global radiomic features for both sarcoidosis subjects and healthy controls. Shading represents 95% confidence intervals, predicted for a female subject, with a mean age of 59.5 years and a mean BMI of 29.0 $kg \cdot m^{-2}$; points represent raw data values per subject, coloured by disease group. The global radiomic features are calculated on the left lung, axial orientation. For the right lung and other orientations, see supplementary tables E2 and E3.

Differences in spatial radiomic measures were noted between sarcoidosis subjects and controls

Radiomic measures differed between sarcoidosis subjects and controls throughout much of the lung across all three planes, as exhibited by separation of confidence bands in figure 3 and t-statistics greater than 1.96 in figure 4. Skewness (top row in figure 3, yellow in figure 4) and kurtosis (second row in figure 3, light

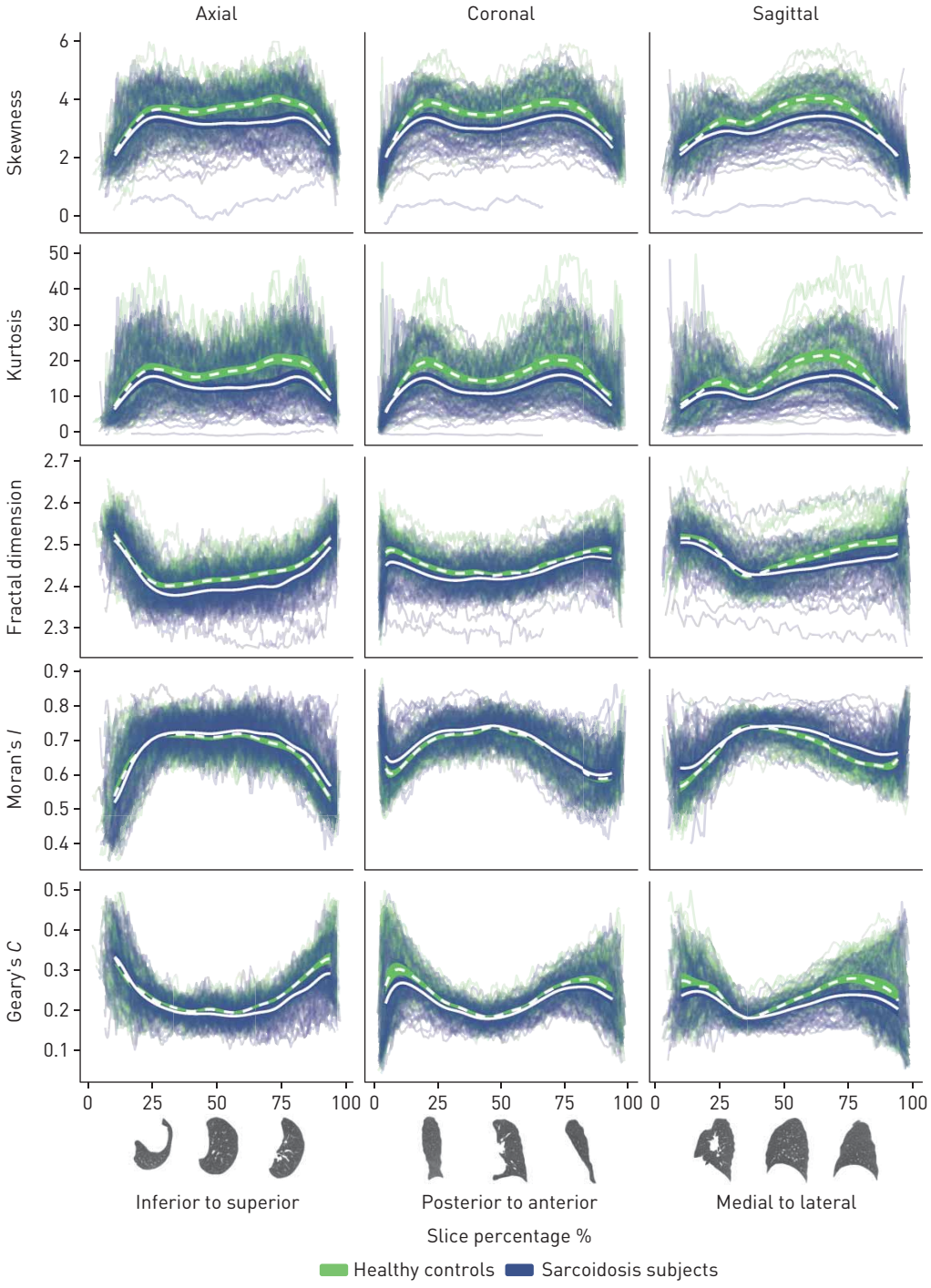

FIGURE 3 Mean radiomic features throughout the lung for sarcoidosis subjects and healthy controls. Shading represents 95% confidence intervals; individual lines represent raw radiomic features throughout the lung per individual, coloured by disease group. Results are shown for the left lung and all orientations. For right lung results, see supplementary figure E1.

green in figure 4) were significantly lower in sarcoidosis subjects compared with controls, with the largest significant differences observed in the superior and middle sagittal lung regions; smaller, but still significant differences were observed in the coronal plane. Fractal dimension (third row in figure 3, teal in figure 4) and Moran's *I* (fourth row in figure 3, dark blue in figure 4) were significantly higher, and Geary's *C* (bottom row in figure 3, dark purple in figure 4) significantly lower, in the sarcoidosis subjects, with the most significant differences in the superior and lateral lung regions; there were also large differences in fractal dimension in the coronal plane. See supplementary figures E1 and E2 for right lung results.

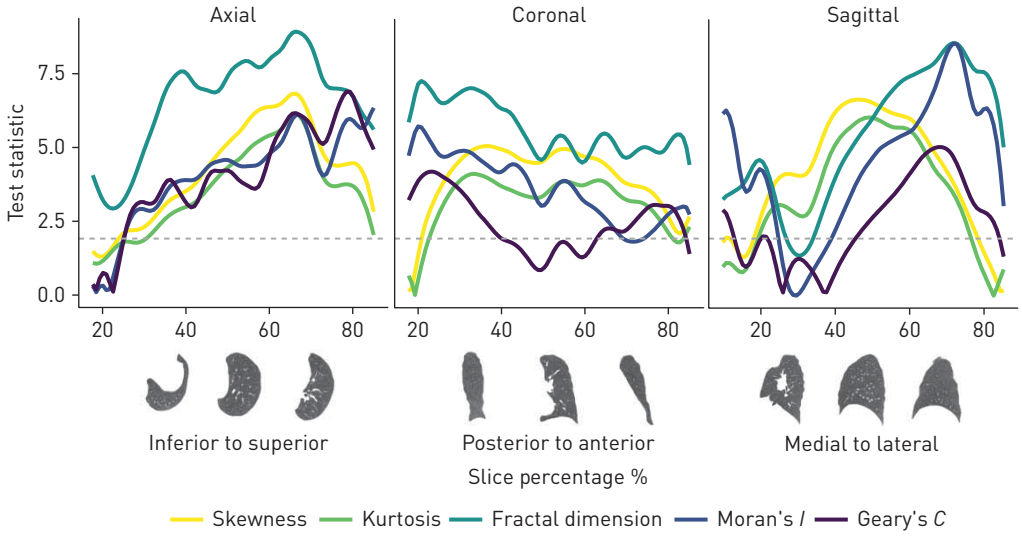

FIGURE 4 Effect size of the absolute difference in radiomic features throughout the lung between sarcoidosis subjects and healthy controls, adjusted for sex, age and body mass index. Assuming a normal approximation, values above 1.96 (dotted line) represent statistically significant differences at a significance level of 0.05. Results are shown for the left lung. For right lung results, see supplementary figure E2.

Radiomic measures of HRCT differed according to Scadding stage classifications

Global radiomic measures differed when patients were classified by Scadding stage, across all anatomical orientations, with the significant differences driven by stage IV (table 3). Not surprisingly, radiomic measures did not follow a sequential increasing or decreasing pattern across Scadding stages. In addition, the various radiomic measures did not follow the same patterns across Scadding stages in terms of which stages have higher (or lower) mean values compared with others. The means of the global skewness, kurtosis and fractal dimension were highest in stage I subjects and lowest in stage IV subjects (p=0.027, p=0.032 and p<0.001, respectively). For the global Moran's *I*, the mean±SE was lowest in stage 0 subjects (0.667±0.013) and highest in stage IV subjects (0.729±0.008) (p<0.001). The mean±SE Geary's *C* was highest in stage III subjects (0.229±0.005) and lowest in stage IV subjects (0.195±0.002) (p<0.001).

Importantly, in sarcoidosis subjects, global radiomic measures explained more variation in the lung function measures than Scadding stage measures. For pre-BD FEV_1, Scadding stage along with sex, age and BMI explained 44.5% of the variability of pre-BD FEV_1 compared with 67.7% with global radiomic measures and sex, age and BMI. Scadding stage along with sex, age and BMI explained 51.4% of the variability in pre-BD FVC, whereas global radiomic measures along with sex, age and BMI explained 71.1% of the variation in pre-BD FVC. For FEV_1/FVC, Scadding stage, sex, age and BMI explained 26.9% compared with 40.2% of the variation explained with global radiomic measures, sex, age and BMI.

Discussion

To the best of our knowledge, this is the first radiomics analysis in sarcoidosis. We show the potential of radiomic measures as biomarkers for sarcoidosis, by 1) detecting differences in HRCT between sarcoidosis subjects and healthy controls, 2) finding associations between radiomic measures and lung function, and 3) identifying trends between Scadding stages. This study can be classified as phase II evidence in the developmental evidence of radiomic measures as biomarkers for sarcoidosis treatment and disease course prediction [24].

In our findings, global radiomic measures differed significantly between sarcoidosis subjects and controls in both the left and right lungs in each anatomical plane. The distribution of Hounsfield units on HRCT from sarcoidosis subjects is more normally distributed (*i.e.* less skew and kurtosis) compared with controls. This is due to increased opacification (*i.e.* whiter areas) on HRCT scans of sarcoidosis subjects, likely caused by parenchymal abnormalities, although it is not clear from our findings which abnormalities are contributing the most. These radiomic findings are consistent with findings *via* visual assessment that note increased opacification and parenchymal abnormalities on HRCT scans from sarcoidosis subjects [2]. Moreover, the significant differences in our second-order radiomic features (fractal dimension, Moran's *I* and Geary's *C*) show adjacent pixels are more similar (in terms of Hounsfield units) on HRCT scans from sarcoidosis subjects compared with controls. This is likely a result of nodule conglomeration and/or fibrosis on HRCT scans of sarcoidosis subjects, which is consistent with findings *via* visual assessment [2].

Furthermore, the spatial radiomic measures displayed significant geographic variation across the lung between sarcoidosis subjects and controls, with differences most apparent in the superior, mid-to-outer sagittal regions. These spatial findings suggest an upper and lateral lobe predominance of radiographic abnormalities in sarcoidosis, which is consistent with findings on visual assessment [35]. Thus, our radiomic findings are consistent with known visual abnormalities for pulmonary sarcoidosis. It is reassuring that these results support rather than conflict with visual scoring. A next step in our work will be to assess correlations between visual assessment and radiomic measures, and to use the two together to provide an integrative radiological assessment of pulmonary sarcoidosis.

Global radiomic measures were also significantly associated with spirometry. The association between radiomic measures and lung function was in general stronger among the sarcoidosis population. In sarcoidosis subjects, lower skewness and kurtosis, likely caused by more parenchymal abnormalities, were associated with lower spirometry. Moreover, lower fractal dimension, higher Moran's *I* and lower Geary's *C*, likely caused by nodule conglomeration and/or fibrosis, were associated with lower spirometry. It is particularly interesting that there are strong associations between radiomic measures and lung function considering that previous work measuring associations between lung function and visual scoring on HRCT scans from sarcoidosis subjects has not shown a consistent association [2]. The associations between radiomic measures and spirometry provide further evidence of the potential clinical utility of radiomic analyses in assessment of pulmonary sarcoidosis.

Based on Scadding stage classifications, we found that global radiomics differed significantly in both the left and right lungs in each anatomical plane, with much of the significant differences driven by Scadding stage IV. For skewness, kurtosis, fractal dimension and Geary's *C*, the most significant pairwise differences were between stage I and IV; for Moran's *I*, between stage 0 and IV. Not surprisingly, radiomic measures did not follow a sequential increasing or decreasing pattern across Scadding stages. In addition, the various radiomic measures did not follow the same patterns across Scadding stages in terms of which stages have higher (or lower) mean values compared with others. These findings are consistent with our knowledge regarding the nonsequential ordering of Scadding stages [2], and the potential for HRCT to provide more sensitive and specific information with regard to parenchymal abnormalities in pulmonary sarcoidosis. Additionally, these radiomic features appear to be sensitive to parenchymal abnormalities noted in Scadding stage IV, such as fibrosis and/or upper lobe volume loss with hilar retraction. Furthermore, we found that radiomic measures are a better predictor of spirometry than Scadding stage, which is consistent with other studies that note the poor predictive ability of Scadding stage with regard to lung function [36, 37].

Further investigation of the utility of radiomic measures as quantitative biomarkers for pulmonary disease, including lung function and other clinical characteristics, is warranted, especially given the ability to generate these measures in an automated fashion. A major benefit of a radiomic analysis is the automated computational efficiency and reproducibility, increasing the potential use of these methods in clinical settings. We analysed 151 segmented scans at ~3 min per scan, which is arguably faster than visual assessment. Radiomic algorithms could be programmed into scanners to be available along with visual reads to further enhance a patient's image profile for sarcoidosis staging and disease monitoring.

Our study is not without limitations. This investigation was performed on a modest sample size. Repeating this analysis in a larger sarcoidosis population will be important to verify generalisability and reproducibility. Based on the way the COPDGene cohort was constructed, our control population was only nonsmokers. We do not believe that this introduced significant biases given the small proportion of smokers in the sarcoidosis population and because a sensitivity analysis removing the sarcoidosis subjects who smoked showed qualitatively similar results to the main results. Although the HRCT scans from both the sarcoidosis subjects and controls were obtained under very similar protocols, we note that a weakness of this study is that the sarcoidosis subjects and controls were scanned on various different Siemens HRCT machines with different tube currents. This potentially introduces biases due to scanner and protocol differences.

To conclude, our work identifies the usefulness of radiomics on HRCT by efficiently and objectively identifying pulmonary parenchymal abnormalities in sarcoidosis subjects. We also highlight the significant association between radiomics and lung function, particularly among those with sarcoidosis, suggesting that the radiomic measures that we evaluated have functional implications. This work shows exciting promise for radiomic measures as biomarkers for disease in sarcoidosis, which should be further evaluated for application in the clinic and/or research setting. We are hopeful that future research with radiomics on HRCT will result in a better understanding of disease progression, classification and treatment options for sarcoidosis subjects.

Acknowledgements: This research used data generated by the COPDGene study, which was supported by NIH grants U01HL089856 and U01HL089897. The COPDGene project is also supported by the COPD Foundation through contributions made by an Industry Advisory Board comprised of Pfizer, AstraZeneca, Boehringer Ingelheim, Novartis, and Sunovion.

Conflict of interest: S.M. Ryan has nothing to disclose. T.E. Fingerlin has nothing to disclose. M. Mroz has nothing to disclose. B. Barkes has nothing to disclose. N. Hamzeh has nothing to disclose. L.A. Maier reports grants from NIH/NHLBI during the conduct of the study, and grants from NIH/NHLBI, aTYR and Mallinckrodt ARD, Inc., outside the submitted work. N.E. Carlson has nothing to disclose.

Support statement: Funding was provided from the US Dept of Health and Human Services, National Institute of Health, National Heart, Lung, and Blood Institute: R01 HL089856, R01 HL114587, R01 HL142049, U01 HL112695 and U01 HL112707. Funding information for this article has been deposited with the Crossref Funder Registry.

An earlier version of this manuscript was posted to ArXiv in June 2018 (arXiv:1806.10281) (https://arxiv.org/abs/1806.10281). Compared with that version, the present manuscript has substantial improvements to its methods, results and presentation.

References

1 Butler MW, Keane MP. Pulmonary sarcoidosis. *Medicine* 2016; 44: 367–372.
2 Nunes H, Soler P, Valeyre D. Pulmonary sarcoidosis. *Allergy* 2005; 60: 565–582.
3 Swigris JJ, Olson AL, Huie TJ, *et al.* Sarcoidosis-related mortality in the United States from 1988 to 2007. *Am J Respir Crit Care Med* 2011; 183: 1524–1530.
4 Valeyre D, Bernaudin J-F, Uzunhan Y, *et al.* Clinical presentation of sarcoidosis and diagnostic work-up. *Semin Respir Crit Care Med* 2014; 35: 336–351.
5 Drent M, De Vries J, Lenters M, *et al.* Sarcoidosis: assessment of disease severity using HRCT. *Eur Radiol* 2003; 13: 2462–2471.
6 Sluimer I, Schilham A, Prokop M, *et al.* Computer analysis of computed tomography scans of the lung: a survey. *IEEE Trans Med Imaging* 2006; 25: 385–405.
7 Keijsers RGM, van den Heuvel DAF, Grutters JC. Imaging the inflammatory activity of sarcoidosis. *Eur Respir J* 2013; 41: 743–751.
8 Nunes H, Uzunhan Y, Gille T, *et al.* Imaging of sarcoidosis of the airways and lung parenchyma and correlation with lung function. *Eur Respir J* 2012; 40: 750–765.
9 Van den Heuvel DA, de Jong PA, Zanen P, *et al.* Chest computed tomography-based scoring of thoracic sarcoidosis: inter-rater reliability of CT abnormalities. *Eur Radiol* 2015; 25: 2558–2566.
10 Jacob J, Bartholmai BJ, Rajagopalan S, *et al.* Mortality prediction in idiopathic pulmonary fibrosis: evaluation of computer-based CT analysis with conventional severity measures. *Eur Respir J* 2017; 49: 1601011.
11 Wormanns D, Kohl G, Klotz E, *et al.* Volumetric measurements of pulmonary nodules at multi-row detector CT: *in vivo* reproducibility. *Eur Radiol* 2004; 14: 86–92.
12 Kumar V, Gu Y, Basu S, *et al.* Radiomics: the process and the challenges. *Magn Reson Imaging* 2012; 30: 1234–1248.
13 Harmouche R, Ross JC, Diaz AA, *et al.* A robust emphysema severity measure based on disease subtypes. *Acad Radiol* 2016; 23: 421–428.
14 Ross JC, Castaldi PJ, Cho MH, *et al.* A Bayesian nonparametric model for disease subtyping: application to emphysema phenotypes. *IEEE Trans Med Imaging* 2017; 36: 343–354.
15 Uppaluri R, Mitsa T, Sonka M, *et al.* Quantification of pulmonary emphysema from lung computed tomography images. *Am J Respir Crit Care Med* 1997; 156: 248–254.
16 Uppaluri R, Hoffman EA, Sonka M, *et al.* Interstitial lung disease: a quantitative study using the adaptive multiple feature method. *Am J Respir Crit Care Med* 1999; 159: 519–525.
17 Hoffman EA, Reinhardt JM, Sonka M, *et al.* Characterization of the interstitial lung diseases via density-based and texture-based analysis of computed tomography images of lung structure and function. *Acad Radiol* 2003; 10: 1104–1118.
18 Ash SY, Harmouche R, Vallejo DLL, *et al.* Densitometric and local histogram based analysis of computed tomography images in patients with idiopathic pulmonary fibrosis. *Respir Res* 2017; 18: 45.
19 Silva AC, Carvalho PCP, Gattass M. Diagnosis of lung nodule using semivariogram and geometric measures in computerized tomography images. *Comput Methods Programs Biomed* 2005; 79: 31–38.
20 da Silva EC, Silva AC, de Paiva AC, *et al.* Diagnosis of lung nodule using Moran's index and Geary's coefficient in computerized tomography images. *Pattern Anal Appl* 2008; 11: 89–99.
21 Wilson R, Devaraj A. Radiomics of pulmonary nodules and lung cancer. *Transl Lung Cancer Res* 2017; 6: 86–91.
22 Lee G, Lee HY, Park H, *et al.* Radiomics and its emerging role in lung cancer research, imaging biomarkers and clinical management: state of the art. *Eur J Radiol* 2017; 86: 297–307.
23 Bashir U, Siddique MM, Mclean E, *et al.* Imaging heterogeneity in lung cancer: techniques, applications, and challenges. *AJR Am J Roentgenol* 2016; 207: 534–543.
24 Pepe MS, Etzioni R, Feng Z, *et al.* Phases of biomarker development for early detection of cancer. *J Natl Cancer Inst* 2001; 93: 1054–1061.
25 Moller DR, Koth LL, Maier LA, *et al.* Rationale and design of the Genomic Research in Alpha-1 Antitrypsin Deficiency and Sarcoidosis (GRADS) study. Sarcoidosis protocol. *Ann Am Thorac Soc* 2015; 12: 1561–1571.
26 Regan EA, Hokanson JE, Murphy JR, *et al.* Genetic epidemiology of COPD (COPDGene) study design. *COPD* 2010; 7: 32–43.
27 Zach J, Newell J, Schroeder J, *et al.* Quantitative CT of the lungs and airways in healthy non-smoking adults. *Invest Radiol* 2012; 47: 596–602.
28 Mackin D, Ger R, Dodge C, *et al.* Effect of tube current on computed tomography radiomic features. *Sci Rep* 2018; 8: 2354.
29 Gneiting T, Ševčíková H, Percival DB. Estimators of fractal dimension: assessing the roughness of time series and spatial data. *Stat Sci* 2012; 27: 247–277.
30 Moran PAP. Notes on continuous stochastic phenomena. *Biometrika* 1950; 37: 17–23.
31 Geary RC. The contiguity ratio and statistical mapping. *Inc Stat* 1954; 5: 115–146.
32 Best AC, Meng J, Lynch AM, *et al.* Idiopathic pulmonary fibrosis: physiologic tests, quantitative CT indexes, and CT visual scores as predictors of mortality. *Radiology* 2008; 246: 935–940.

33 Tanabe N, Muro S, Sato S, *et al.* Fractal analysis of low attenuation clusters on computed tomography in chronic obstructive pulmonary disease. *BMC Pulm Med* 2018; 18: 144.
34 Green PJ, Sliverman BW. Nonparametric Regression and Generalized Linear Models: A Roughness Penalty Approach. Boca Raton, CRC Press, 1993.
35 Lynch JP III. Computed tomographic scanning in sarcoidosis. *Semin Respir Crit Care Med* 2003; 24: 393–418.
36 Stanojevic S, Wade A, Stocks J, *et al.* Reference ranges for spirometry across all ages: a new approach. *Am J Respir Crit Care Med* 2008; 177: 253–260.
37 Statement on Sarcoidosis. Joint Statement of the American Thoracic Society (ATS), the European Respiratory Society (ERS) and the World Association of Sarcoidosis and Other Granulomatous Disorders (WASOG) adopted by the ATS Board of Directors and by the ERS Executive Committee, February 1999. *Am J Respir Crit Care Med* 1999; 160: 736–755.